# Copper-catalysed glutathione oxidation is accelerated by the anticancer thiosemicarbazone Dp44mT and further boosted at lower pH

Enrico Falcone,[a,#] Alessandra G. Ritacca,[b,#] Sonja Hager,[c] Bertrand Vileno,[a] Youssef El Khoury,[d] Petra Hellwig,[d] Christian Kowol,[e] Petra Heffeter,[c] Emilia Sicilia,[b,*] Peter Faller[a,f,*]

[a] Institut de Chimie (UMR 7177), University of Strasbourg – CNRS, 4 Rue Blaise Pascal, 67081 Strasbourg, France.

[b] Department of Chemistry and Chemical Technologies, Università della Calabria, Ponte P. Bucci, 87036 Arcavacata di Rende (CS), Italy.

[c] Center for Cancer Research, Medical University of Vienna, Borschkegasse 8a, 1090 Vienna, Austria

[d] Laboratoire de bioélectrochimie et spectroscopie, UMR 7140, CNRS, Université de Strasbourg, 4 Rue Blaise Pascal, 67081 Strasbourg, France

[e] Institute of Inorganic Chemistry, Faculty of Chemistry, University of Vienna, Waehringer Straße 42, 1090 Vienna, Austria.

[f] Institut Universitaire de France (IUF), Paris, France

[#] These authors contributed equally

* corresponding authors: pfaller@unistra.fr (P. F.), emilia.sicilia@unical.it (E. S.)

**Abstract**

Glutathione (GSH) is the most abundant thiol in mammalian cells and plays a crucial role in maintaining the redox state of many biomolecules, in detoxification and antioxidant defence. The thiols of two GSH molecules can be oxidized to the disulphide GSSG. The cytosolic GSH/GSSG ratio is very high (> 100), and its decrease can lead to apoptosis or necrosis, which are of interest in cancer research. $Cu^{II}$ ions are very efficient oxidants of thiols, but with an excess of GSH, the formed $Cu^{I}_{n}(GS)_{m}$ clusters are only slowly re-oxidized by $O_2$ at pH 7.4, and even more slowly at lower pH. Here, the oxidation of GSH by $Cu^{II}$ was investigated in the presence of the anticancer thiosemicarbazone Dp44mT. The results showed that $Cu^{II}$-Dp44mT oxidizes GSH faster than $Cu^{II}$ alone at pH 7.4, and hence accelerates the production of the very reactive hydroxyl radicals. Interestingly, GSH oxidation and hydroxyl radical production by $Cu^{II}$-Dp44mT were accelerated at the acidic pH found in lysosomes, where $Cu^{II}$-Dp44mT was previously shown to accumulate and induce lysosomal membrane permeabilization. To decipher this unusually faster thiol oxidation at lower pH, Density Functional Theory (DFT) calculations and spectroscopic studies were performed. The results suggest that the acceleration is due to the protonation of $Cu^{II}$-Dp44mT on the hydrazinic nitrogen, which favours the rate-limiting reduction step without subsequent dissociation of the $Cu^{I}$-complex. Furthermore, preliminary biological studies in cell culture using the proton pump inhibitor bafilomycin A1 indicated that the lysosomal pH plays a role in the activity of Dp44mT.

## Introduction

Glutathione (γ-glutamyl-cysteinyl-glycine, GSH) is one of the highest concentrated biomolecules and the most abundant (0.5–15 mM) low-molecular-weight thiol in mammalian cells. The reduced/oxidized glutathione (GSH/GSSG) couple is the main intracellular regulator of redox homeostasis in animals and plants. Under physiological conditions, most GSH is present in the reduced state, exceeding a GSH:GSSG ratio of 1000:1 in cytosol and nucleus, whereas a shift to a lower value of this ratio leads to apoptosis or necrosis.[1] GSH has several important roles: control of the thiol oxidation state of proteins, defence against oxidative stress, and detoxification. It also acts as an antioxidant, both by directly scavenging reactive oxygen species (ROS) and by repairing their damage via enzymatic processes. Thus, GSH is a crucial compound for living cells and targeting GSH metabolism is of wide interest for therapeutic purposes, in particular for fighting cancer.[2]

Indeed, cancer cells often have high GSH concentrations and elevated GSH levels are indicative of tumour progression and increased drug resistance.[3] Depletion of GSH, then, is considered to be a promising anticancer strategy, in particular in combinatorial approaches.[4]

In general, thiols can be oxidized to disulfides under aerobic conditions according to the following reaction:

$$2\ RSH \rightarrow RSSR + 2\ H^+ + 2\ e^- \qquad \text{(i)}$$

Under aerobic conditions, this is a spontaneous reaction, and the cystine/cysteine couple has a quite low standard redox potential of about -0.22 V at pH 7 vs. SHE,[5] while for the GSSG/GSH couple it is slightly lower, -0.26 V,[1] at the same pH. According to the Nernst equation, the redox-potential increases by 59 mV per pH unit below the $pK_a$. Hence, reaction (i) becomes more and more thermodynamically unfavourable as the pH decreases. Beside the thermodynamic driving force, the kinetics of thiol oxidation is also slowed down by lowering the pH. In addition, the so-called thiol-disulfide exchange, the redox reaction between thiols and disulfides, is also slowed down at decreasing pH. Thus, lowering the pH is an approach used to quench thiol oxidation and disulfide exchange reactions. The lower reactivity of thiols at lower pH is generally attributed to the significantly higher reactivity of thiolates compared to thiols. Thiolates are, indeed, better nucleophiles and, hence, react quickly with electrophiles like disulfide bonds, $O_2$, $H_2O_2$, other ROS, metal ions etc. Whereas some thiols react rapidly, GSH oxidation is quite sluggish at pH 7 and the activity drops notably by lowering the pH.[6] Moreover, the $pK_a$ value of a thiol is crucial in determining its reactivity, as demonstrated by the higher reactivity of Cys ($pK_a$ ~8.3) compared to GSH ($pK_a$ ~9).[6] This higher $pK_a$ and the correlated lower reactivity might explain why GSH and not

Cys is the main low-molecular-weight thiol in cells. Indeed, cells spend high energetic efforts to avoid non-specific thiol reactions allowing a better control of other metabolically relevant thiol reactions. Copper and, to a lesser extent, iron are able to catalyse the oxidation of thiols by $O_2$.[6] Although the precise mechanism of $Cu^{II}$-catalysed thiol oxidation has not been unambiguously ascertained, it supposedly involves the formation of a thiolate-$Cu^{II}$ ($RS^-$-$Cu^{II}$) complex accompanied by thiol deprotonation (ii), the inner-sphere electron transfer from the thiol to $Cu^{II}$ forming $Cu^{I}$ and a thiyl radical $RS^{\bullet}$ (iii), the combination of two $RS^{\bullet}$ radicals forming the disulfide RSSR (iv), and the re-oxidation of $Cu^{I}$ to $Cu^{II}$ by $O_2$ with the formation of a superoxide radical anion, $O_2^{\bullet-}$ (v).[7]

$$2\ RSH + Cu^{II} \rightarrow RS^{-}\text{-}Cu^{II} + H^{+} \qquad \text{(ii)}$$

$$RS^{-}\text{-}Cu^{II} \rightarrow RS^{\bullet}\text{-}Cu^{I} \qquad \text{(iii)}$$

$$2\ RS^{\bullet}\text{-}Cu^{I} + n\ RS^{-} \rightarrow RSSR + Cu^{I}\text{-}(RS^{-})_n \qquad \text{(iv)}$$

$$Cu^{I}\text{-}(RS^{-})_n + O_2 \rightarrow Cu^{II}\text{-}(RS^{-})_n + O_2^{\bullet-} \qquad \text{(v)}$$

In alternative to reactions (ii) and (iii), a disulfide radical anion, $RS^{\bullet-}$–SR, could be formed and then oxidised to the disulfide RSSR.

In the present combined experimental and computational study, we report on the very surprising faster GSH oxidation under aerobic conditions at lower pH together with the attempts to decipher the mechanistic aspects of the oxidation reaction. Such a faster GSH oxidation is catalysed by the $Cu^{II}$ complex with the anticancer α-pyridyl thiosemicarbazone (TSC) Dp44mT (di-2-pyridylketone-4,4-dimethyl-3-thiosemicarbazone, see Chart 1). This observation is not only of chemical interest, as it concerns the efficient thiol oxidation at lower pH but also has a biological and medicinal impact. Indeed, Dp44mT, whose derivatives DpC and COTI-2 entered phase I clinical trials in cancer research (see Chart 1),[8] showed a pronounced synergism with $Cu^{II}$, suggesting the involvement of Cu chelation in the mode of action, and $Cu^{II}$-Dp44mT was able to reduce the cellular GSH/GSSG ratio, possibly via the generation of ROS.[9]

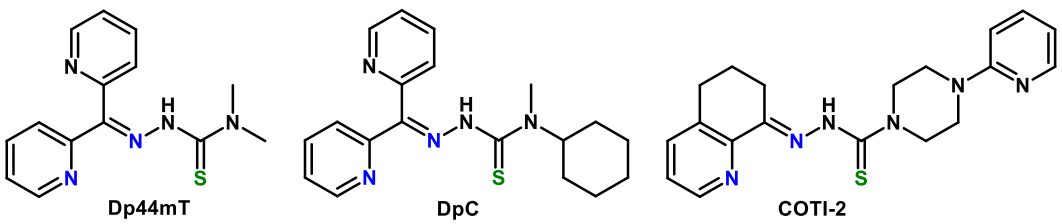


**Chart 1**. Structures of Dp44mT and its clinically-relevant derivatives DpC and COTI-2.

Interestingly, $Cu^{II}$-Dp44mT seems to localize in compartments with lower pH such as lysosomes.[9, 10] Moreover, $Cu^{II}$-Dp44mT is able to inhibit the ER-resident enzyme protein disulfide isomerase (PDI), which has been hence proposed as a potential target of certain $Cu^{II}$-TSC complexes in cancer cells. Likely, $Cu^{II}$-TSC might interfere with PDI function through the binding and/or oxidation of essential cysteine residues.[11]

α-Pyridyl TSCs are tridentate ligands forming square-planar $Cu^{II}$-complexes. Depending on the pH, two Cu-bound species may exist, namely $Cu^{II}$-**H**TSC and $Cu^{II}$-TSC, which differ in the protonation state of the non-coordinating hydrazinic ($N^2$) nitrogen (see equilibrium iv in Scheme 1) and for the character of the S donor. Indeed, upon $N^2$ deprotonation, the thione-thiol tautomerism shifts towards the negatively charged thiolate form (see equilibrium ii, Scheme 1). Generally, such ($N_{py}$, N, $S^-$) coordination mode predominates at pH > ~3.[12]

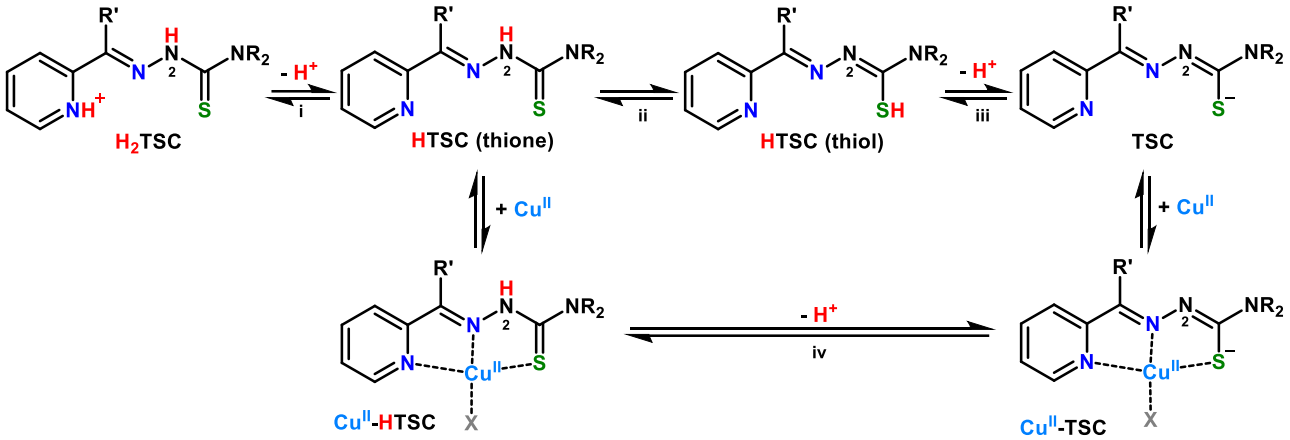


**Scheme 1.** Protonation equilibria of TSCs and their $Cu^{II}$-complexes: (i) (de)protonation of α-pyridyl nitrogen; (ii) thione-thiol tautomerism; (iii) (de)protonation of the thioamide moiety; (iv) (de)protonation of the hydrazinic nitrogen in the Cu-complex.

Moreover, $Cu^{II}$-TSCs complexes have negative reduction potentials (~ –0.2 V vs. NHE) since the imposed square-planar geometry is rather unsuited for $Cu^{I}$ binding. As a result, $Cu^{II}$-TSC complexes are not reduced by ascorbate even in large excess, in line with the higher redox potential of ascorbate.[13, 14] Similarly, $Cu^{II}$-Dp44mT and its analogues, unlike other TSC complexes, also withstand the reductive dissociation by GSH under anaerobic conditions.[14]

## Results and discussion

*Reaction of $Cu^{II}$-Dp44mT and GSH at pH 7.4*

The interaction between $Cu^{II}$-Dp44mT and GSH under aerobic conditions was first investigated via UV-vis absorption spectroscopy. Consistently with previous reports, $Cu^{II}$-Dp44mT appears to be resistant to the dissociation by the thiol, forming a ($GS^-$)-$Cu^{II}$-Dp44mT ternary complex, as indicated by the steady red-shifted S→$Cu^{II}$ charge transfer (CT) absorption band at 412 nm (see Figure S1A).[15] We further confirmed the formation of such a ternary complex using experimental and simulated Raman spectra (see Figure S2), where the ν(Cu-N) vibration, as predicted by simulations, downshifts from 551 $cm^{-1}$ for the $Cu^{II}$-Dp44mT to 546 $cm^{-1}$ upon $GS^-$ binding.

However, despite the apparent stability of this ternary complex over time, we observed a gradual increase in the absorbance at ~254 nm (see Figure S1A). This band may arise from the formation of glutathione disulfide (GSSG) upon transient $Cu^{II}$ reduction by GSH and re-oxidation by $O_2$ (see Figure S1C and reactions vi and vii):

$$Cu^{II}\text{-Dp44mT} + 2\ GSH \rightarrow [Cu^{I}\text{-Dp44mT}] + GSSG + 2\ H^+ \quad \text{(vi)}$$

$$[Cu^{I}\text{-Dp44mT}] + O_2 \rightarrow Cu^{II}\text{-Dp44mT} + O_2^{\bullet -} \quad \text{(vii)}$$

Indeed, the observed absorbance increase roughly matches the conversion of 3 mM GSH to 1.5 mM GSSG ($\varepsilon_{248}$ = 380 $M^{-1}cm^{-1}$).[16] In order to assess whether the absorbance increase at 254 nm corresponds to GSH oxidation, we monitored the reaction by HPLC, confirming the formation of GSSG and the consumption of GSH (see Figure S3A). The good correlation between the spectral change at 254 nm and the HPLC peak area corroborated the attribution of the band at 254 nm to GSSG (see Figure S4). Of note, spectroscopic and HPLC analysis also showed that the $Cu^{II}$-Dp44mT oxidised GSH faster than $Cu^{II}$ only (see Figure S5).

*Reaction of $Cu^{II}$-Dp44mT and GSH at pH 5.0*

Next, owing to the co-accumulation of Dp44mT and $Cu^{II}$ in lysosomes observed by Richardson *et al.*,[9, 10] we also investigated the interaction of $Cu^{II}$-Dp44mT and GSH at pH 5. Raman spectra confirm the binding of GSH to the $Cu^{II}$-Dp44mT at pH 5 (see Figure S1B). The time-dependent UV-vis spectra of the mixture showed the partial and transient decrease of the CT band at ~412 nm, and the concurrent increase of the absorbance at 254 nm (see Figure S1B). Surprisingly, such an increase was faster at pH 5 than at pH 7.4 (see Figure 1A). Likewise, HPLC analysis revealed that GSH oxidation to GSSG was faster at pH 5 than 7.4. (see Figure 1B and S3B).

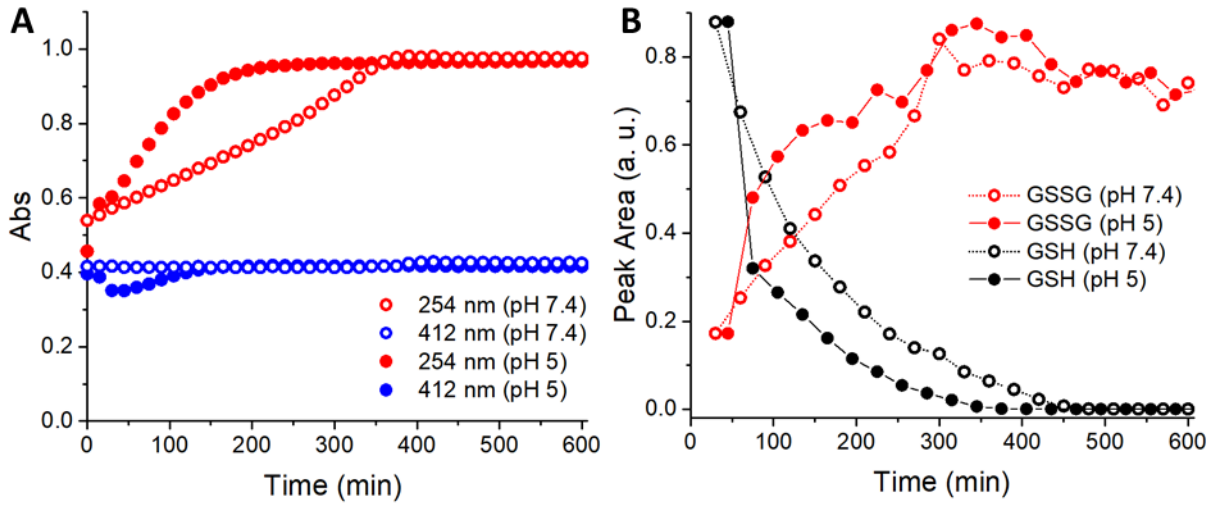


**Figure 1.** (A) Absorbance changes at 254 nm (red) and 412 nm (blue) upon interaction of $Cu^{II}$-Dp44mT with GSH at pH 7.4 (empty circle) and 5 (full circle). (B) GSH oxidation to GSSG followed by HPLC. Conditions: [$Cu^{II}$] = 27 µM, [Dp44mT] = 30 µM, [GSH] = 3 mM; buffer: 100 mM HEPES pH 7.4 or 100 mM MES pH 5; DMSO 2%.

Besides, as GSH oxidation by $Cu^{II}$-Dp44mT is associated with $O_2$ reduction to ROS, we evaluated the generation of the HO• radical via electron paramagnetic resonance (EPR) spectroscopy using TEMPOL (4-hydroxy-2,2,6,6-tetramethylpiperidin-1-oxyl) as a radical scavenger (the EPR signal of the stable nitroxyl TEMPOL radical is quenched upon reaction with radicals such as HO•).[17] Thus, we also observed a ~ 4-fold faster HO• production at pH 5 than at pH 7.4 (see Figure 2). In contrast, the HO• production and the GSH oxidation by $Cu^{II}$ in absence of an added $Cu^{II}$-ligand are slowed down at lower pH (see Figures 2 and S6).[18]

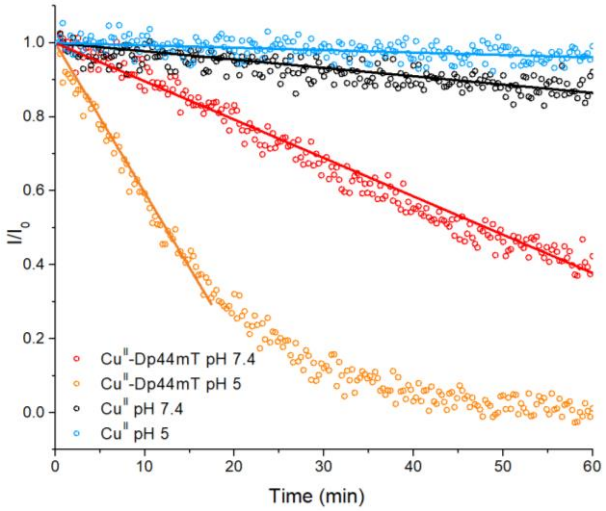


**Figure 2.** Decay of TEMPOL EPR signal in the presence of $Cu^{II}$-Dp44mT or $Cu^{II}$ and GSH at pH 7.4 or 5. Conditions: [$Cu^{II}$] = 27 µM, [Dp44mT] = 30 µM, [GSH] = 3 mM, $[TEMPOL]_0 = I_0$ = 20 µM; buffer: 100 mM HEPES pH 7.4 or 100 mM MES pH 5, DMSO 2% (in the presence of Dp44mT). The initial decay of TEMPOL EPR intensity (solid lines) was linearly fitted to estimate the HO• production rate (slope of the fitted curves).

To get insights into the observed pH dependence, we also studied the reduction of $Cu^{II}$-Dp44mT by GSH in anaerobic conditions (Figure S7) and found it to be faster at lower pH. As the ($GS^-$)-$Cu^{II}$-Dp44mT species is observed throughout the reaction in presence of $O_2$, the oxidation of $Cu^I$ by $O_2$ (reaction vii) is faster than the reduction of $Cu^{II}$ by GSH (reactions vi) and, hence, ($GS^-$)-$Cu^{II}$-Dp44mT appears to be constant. Therefore, reduction seems to be the rate-limiting step and lowering the pH accelerates this step. Such observations appear very surprising and puzzling since, as mentioned above, the rate of thiol oxidation is normally much slower at lower pH due to the lower reactivity of thiol compared to thiolate. Hence, we posit that different pH-dependent speciation of the $Cu^{II}$-Dp44mT complex, rather than the thiol reactivity, is accountable for the unusual pH-dependent behaviour observed.

*DFT calculations*

In order to investigate the mechanism of the reaction between $Cu^{II}$-Dp44mT and GSH and in an attempt to rationalize the unexpected pH-dependent behaviour, we performed quantum-mechanical Density Functional Theory (DFT) calculations. The sequence of steps that leads to $Cu^{II}$-Dp44mT reduction by GSH was investigated using L-cysteine (Cys) as a thiol model to reduce the required computational efforts. On the basis of the experimental findings showing that at physiological pH, the Dp44mT ligand is deprotonated on the hydrazinic $N^2$ atom (see Scheme 1) when coordinated to $Cu^{II}$,[14] calculations were carried out considering the complex in its deprotonated form $Cu^{II}$-Dp44mT with a water molecule occupying the fourth position of the nearly square planar geometry (see **React** in Scheme 2).

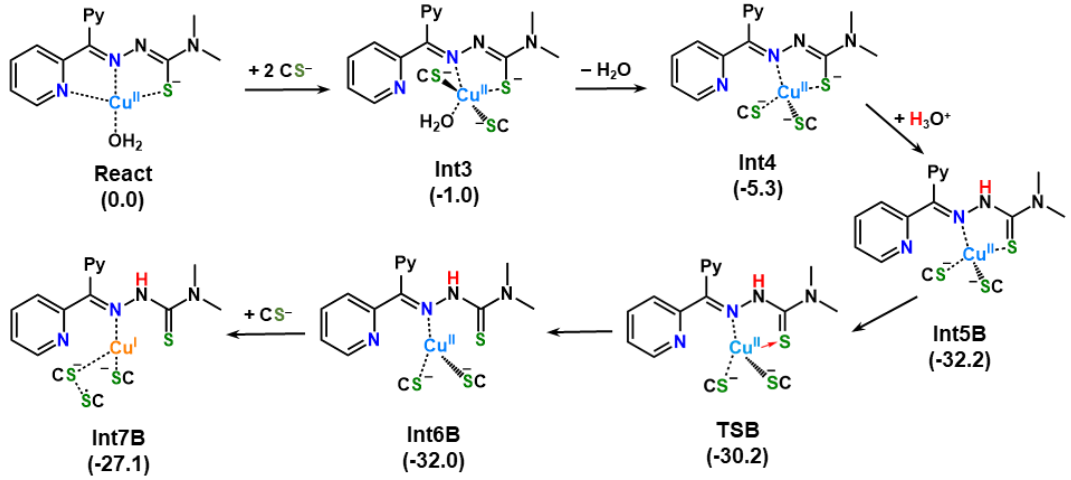


**Scheme 2.** Main steps of the DFT-calculated mechanism of $Cu^{II}$-Dp44mT reduction in the presence of three deprotonated cysteines. The relative Gibbs free energies ($\Delta G^{298K}$) are given in brackets in kcal/mol. In the transition state (TSB connecting the minima **Int5B** and **Int6B**) a red arrow represents the detachment of the ligand S from the Cu ion.

The main steps describing the mechanism of the reaction are reported in Scheme 2. The starting $Cu^{II}$-(Dp44mT)($H_2O$) complex plus three deprotonated cysteines, $Cys^-$, was set as the reference zero energy for calculating relative Gibbs free energies, $\Delta G^{298K}$. Fully optimized geometrical structures of the located stationary points are collected in Figure S8. The first adduct, **Int1**, formed between $Cu^{II}$-Dp44mT and one approaching $Cys^-$, which is more stable than the separated reactants by 7.7 kcal/mol, is characterized by electrostatic interaction between both the thiol sulfur and one of the carboxylate oxygen atoms with the water hydrogens (see Figure S8). One of two other $Cys^-$ coordinates to Cu forming the **Int2** adduct, only slightly more stable, by 1.1 kcal/mol, than the previous one (see Figure S8). Owing to the coordination of a second $Cys^-$, a pseudo square pyramidal structure is adopted by the complex **Int3** (see Scheme 2 and Figure S8), lying below the reference energy of the separated reactants by 1.0 kcal/mol.

Simultaneously, the bonds with the pyridine nitrogen $N_{py}$ and the water molecule elongate preluding to their definitive detachment that occurs in the next minimum **Int4,** accompanied by a further stabilization of 4.3 kcal/mol (see Scheme 2 and Figure S8). All these reorganizations occurring in presence of $Cys^-$ units do not involve any electron transfer. The **Int4** adopts a pseudo-tetrahedral geometry and the Dp44mT ligand continues to be firmly bound to the copper centre in a bidentate fashion through the N and S atoms, even if the bond with the ligand S atom is longer than in the tridentate coordination (see Scheme 2). It is also noteworthy that the third $Cys^-$ does not get involved in any interaction with the Cu centre. All the attempts to trigger a rearrangement leading from $Cu^{II}$ reduction to $Cu^{I}$ failed as we proved performing a spin density analysis. Latter showed that the reduction was only accomplished by manually detaching the ligand from Cu, leading to the **Int5A** product (see Figure S8 and S9), whose formation is thermodynamically disfavoured (less stable than the separated reactants by 12.4 kcal/mol) and is not connected to the preceding minimum through either a spontaneous reorganization or a transition state.

Motivated by the outcomes of preliminary calculations performed for the protonated form of the complex, $Cu^{II}$-**H**Dp44mT, and by the hypothesis formulated on the basis of the experimental findings illustrated above, we have explored the possibility that the Cu reduction is driven by the re-protonation of the hydrazinic $N^2$ nitrogen (see Scheme 2). Indeed, the $N^2$ protonation shifts the character of the S donor from thiolate to the weaker thione (see equilibrium ii in Scheme 1) and hence may favour the S de-coordination forming a non-planar intermediate more prone to $Cu^{II}$ reduction. Interestingly, the importance of such a partial de-coordination on the reduction of $Cu^{II}$ by GSH was recently shown with the tridentate peptide ligand GHK.[19]

To this aim, considering that the $Cu^{II}$-Dp44mT complex can exist in equilibrium with its protonated form $Cu^{II}$-**H**Dp44mT in solution (see Scheme 1), we have simulated the re-protonation of the $N^2$ atom

(see Scheme 1) using a hydronium ion as a protonating agent. Thus, the reaction proceeds as shown in Scheme 2. After the addition of an $H_3O^+$ unit to the **Int4** minimum, which causes a spontaneous transfer of a proton to the $N^2$ atom while the formed water molecule establishes a hydrogen bond with the transferred proton, the new optimized minimum (**Int5B**) is formed with a release of 32.2 kcal/mol with respect to the energy of the entrance channel, reset to include the energy of an additional $H_3O^+$ unit. No other significant reorganization of the complex molecular structure takes place. In the effort to find a path leading to the formation of a $Cu^I$ species, the very numerous used computational strategies converged on a transition state, **TSB** in Scheme 2, lying 30.2 kcal/mol below the reference zero energy, that allows the definitive detachment of the Dp44mT ligand S atom. Formation of the next intermediate **Int6B**, obtained overcoming an energy barrier of 2.0 kcal/mol is almost thermoneutral with respect to the previous minimum. Finally, the presence of the third $Cys^-$ enables the reduction of Cu, obtaining a product (**Int7B**) which is less stable than the preceding minimum by only 4.9 kcal/mol. In particular, $Cu^I$ results to be linearly coordinated by the hydrazinic $N^2$ atom of the **H**-Dp44mT ligand and the S atom of the equatorial Cys, while the bond with the axial $Cys^-$ weakens due to the formation of a sort of adduct with the unbound $Cys^-$. Indeed, as shown in Figure 3, the spin density distribution of the unpaired electron is shared by the two unbound Cys.

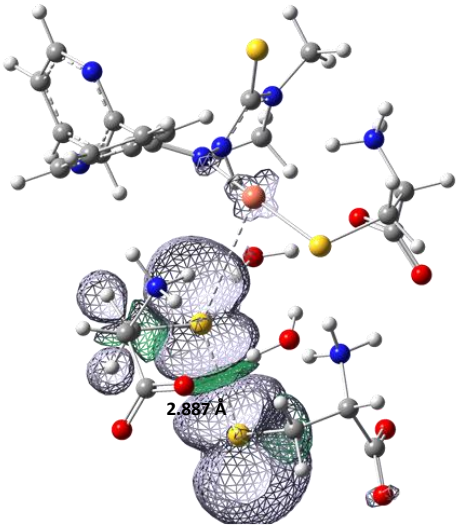


**Figure 3.** Electronic spin density plot for the product **Int7B**. The value of the calculated S-S distance is also reported.

Hence, it seems that the axial $Cys^-$ acts as a bridge that allows the transfer of one electron from the unbound $Cys^-$ to the Cu ion. Remarkably, the need for a third Cys to accomplish the Cu reduction, as well as the final spin density distribution, suggests that the reduction process involves the formation of a disulfide radical anion ($RS^{\bullet -}$–SR) rather than a thiyl radical ($RS^{\bullet}$)[20] as the intermediate. This is also supported by the close similarity between the S-S distance in the **Int7B** adduct, namely 2.887 Å,

and the reported S-S bond length (~2.8 Å) in disulfide radical anions.[21] It is also worth noting that a similar disulfide radical adduct is observed in **Int5A** (see Figures S8 and S9).

Besides, it is important to underscore that, in spite of the reduction of the Cu centre, the Dp44mT ligand continues to be partially coordinated to the metal.[14] This is consistent with the high stability of the complex against the dissociation by GSH and corroborates the hypothesis that the formed $Cu^{I}$ intermediate can be easily re-oxidized in the presence of $O_2$. On balance, our computational analysis suggests that the protonation of the hydrazinic $N^2$ nitrogen is required for the reduction to occur.

*pH-dependent speciation of $Cu^{II}$-Dp44mT*

The hypothesis that the reduction is fostered by different pH-dependent speciation of the $Cu^{II}$-Dp44mT complex, rather than from the reducing power of the thiol, is supported by the calculated mechanism of reaction (Scheme 2), in which the $Cu^{I}$ complex is formed only after the protonation of the hydrazinic $N^2$ atom of the ligand.

Therefore, to get insight into the speciation of $Cu^{II}$-Dp44mT as a function of the pH, we performed a spectrophotometric pH titration of the $Cu^{II}$-Dp44mT complex (see Figure 4).

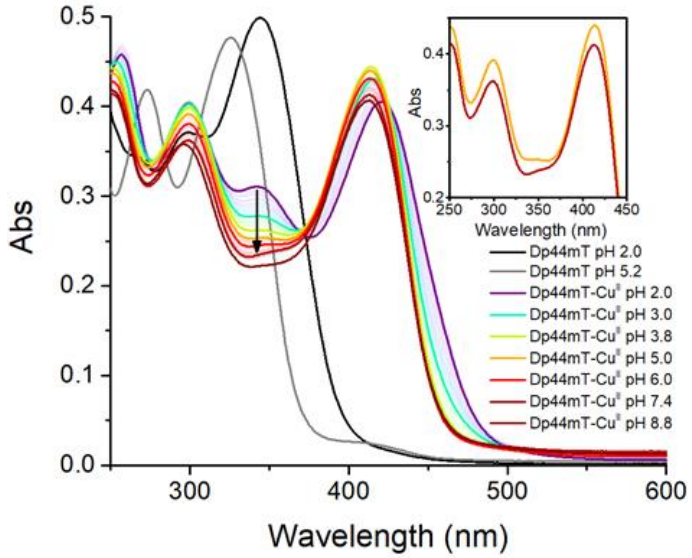


**Figure 4.** Spectrophotometric pH titration of $Cu^{II}$-Dp44mT; inset: comparison of the spectra at pH 5 (orange) and 7.4 (red). Conditions: [$Cu^{II}$] = 27 µM, [Dp44mT] = 30 µM; DMSO 2%. The black arrow highlights the decrease of the band at ~345 nm with the increasing pH.

At pH 2, a band at ~345 nm can be clearly distinguished. Interestingly, this band decreased when increasing the pH and hence it can be attributed to the protonated $Cu^{II}$-**H**Dp44mT complex. Note that, although the Cu-free doubly-protonated ligand (**$H_2$**Dp44mT, with the second proton at the non-coordinating pyridyl moiety) also absorbs at ~344 nm, this species is absent at pH 5 (see Figure 4 and S10). In addition, we calculated the UV-vis spectra of the $N^2$-protonated and deprotonated forms of

the complex using the time-dependent extension of DFT (see Figure S11). As it is evident, the peak in the computed spectrum of the protonated form of the complex appearing at 343 nm is absent in the spectrum of the deprotonated form, in good agreement with experimental spectra.

Furthermore, considering the $pK_a$ of 2.34 previously reported for the $Cu^{II}$-**H**Dp44mT complex[14], as well as the computed extinction coefficient for the band at 343 nm (~ 25000 $M^{-1}cm^{-1}$), we estimated the portion of $N^2$-protonated $Cu^{II}$-**H**Dp44mT species to be as low as ~ 0.2% at pH 5. In light of the proposed mechanism involving the transient protonation of the intermediate (**Int5**), such a minor yet significant portion of $N^2$-protonated form at pH 5 may account for the faster GSH oxidation. Moreover, we speculate that the addition of a negatively charged $GS^-$ unit to Cu coordination sphere may increase the $pK_a$ of the hydrazinic nitrogen and hence increase the population of the $N^2$-protonated species. Indeed, based on DFT calculations, the $N^2$-protonation of the Cys-bound **Int4** complex results to be more favourable (by ~12 kcal/mol) than that of the water-bound **React** species. Besides, to assess the influence of the non-coordinating pyridyl moiety, whose $pK_a$ is nevertheless very low (< 2),[14] we examined the behaviour of some Dp44mT analogues devoid of such pyridyl group, namely Ap44mT and PTSC (see Figure S12). These compounds also showed a faster GSH oxidation at lower pH, proving that the pyridyl moiety in Dp44mT has little, if any, influence on such pH dependence (see Figure S12).

*Significance of lysosomal pH for the cell toxicity of Dp44mT*

Based on the higher reactivity of $Cu^{II}$-Dp44mT at lower pH and considering its accumulation in lysosomes (see above), we wondered if increasing the pH of the lysosomes influences the toxicity of Dp44mT. To address this question, we utilized bafilomycin A1 (BafA1), an inhibitor of the $H^+$-pump responsible for the acidification of lysosomes.[22] Briefly, SW480 cells were incubated with BafA1 for 1 h, followed by the addition of Dp44mT or its copper complex for 48 h. After this co-incubation, cell viability was analysed by MTT assay as indicated in the experimental section. In general, the activity of the $H^+$-pump is crucial for cell functionality. Consequently, the long-term treatment with BafA1 was rather toxic to SW480 cells (~32% at the highest concentration of BafA1, see Figure S13). However, BafA1 treatment had strong antagonistic activity (combination index values above 1) and was able to protect SW480 cells from treatment with Dp44mT or its copper complex (see Figure 5). Interestingly, these effects were more pronounced upon treatment with the copper complex than with the metal-free Dp44mT. These preliminary experiments indicate that, indeed, the acidification of the lysosomes plays a role in the biological activity of $Cu^{II}$-Dp44mT.

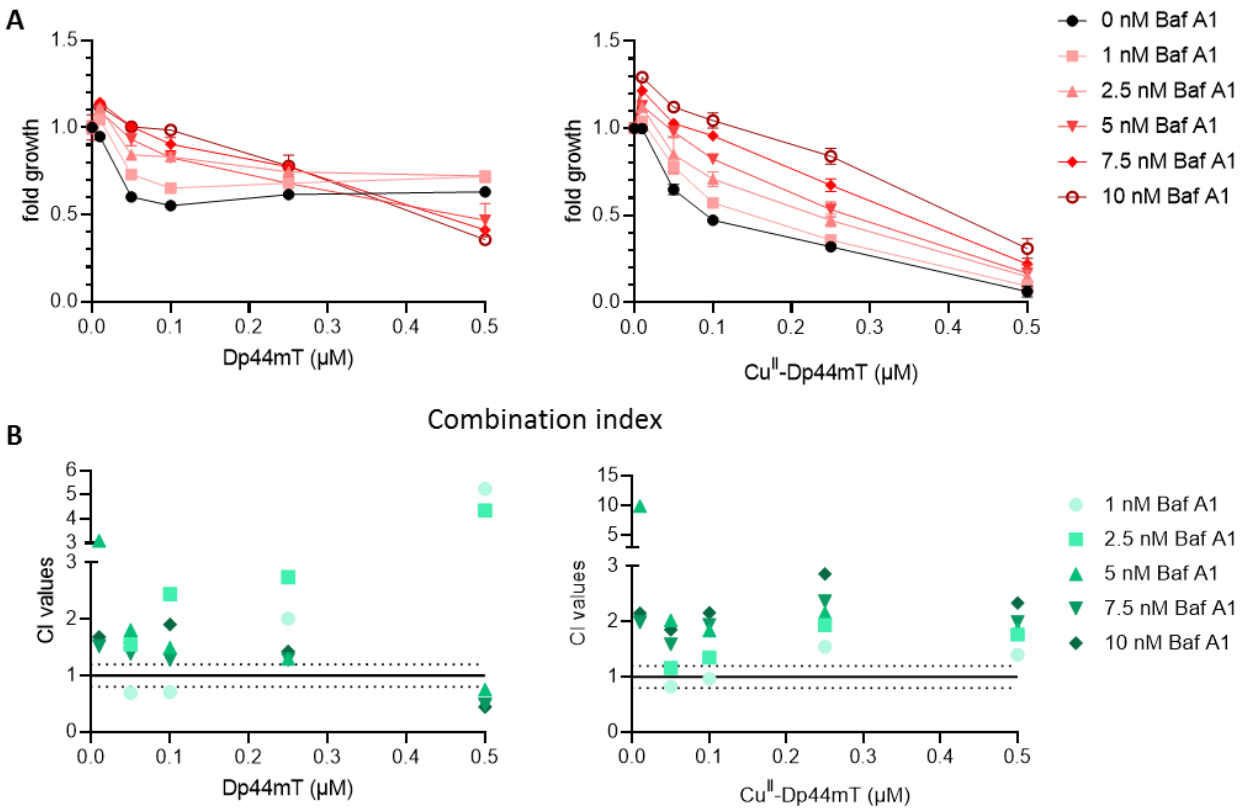


**Figure 5.** Effect of bafilomycin A1 (BafA1) on viability of SW480 cells treated with Dp44mT or its copper complex with indicated concentrations for 48 h. A) Viability was measured by MTT viability assays. Values given are mean ± standard deviation (SD) derived from triplicates of one representative experiment out of three and normalized to cells treated with respective concentration of BafA1 alone. B) Combination indices were calculated by CalcuSyn. Combination (CI) values above 1 indicate antagonism and values below 1 synergism.

## Conclusions

The faster oxidation of GSH by $O_2$ in the presence of $Cu^{II}$-Dp44mT at pH 5 compared to pH 7.4 is quite remarkable. Generally, the reactivity of thiols slows down with lowering the pH, because deprotonated thiolates are the most reactive form. Indeed, GSH oxidation by $Cu^{II}$ only, already slower than $Cu^{II}$-Dp44mT at pH 7.4, further decelerates at pH 5. Hence, the catalytic activity of $Cu^{II}$-Dp44mT compared to $Cu^{II}$ only is even more remarkable at pH 5. GSH reduces $Cu^{II}$ rapidly to form $Cu^{I}_{n}(GS^{-})_{m}$ clusters,[23] whose re-oxidation by $O_2$ is slow and rate-limiting.[24] In contrast, in line with the square-planar coordination via 5-membered chelate rings favouring $Cu^{II}$, the reduction seems to be the rate-limiting step for $Cu^{II}$-Dp44mT. Accordingly, an important feature for the efficient GSH oxidation in the case of $Cu^{II}$-Dp44mT is to withstand the dissociation by GSH, which has a quite high affinity for $Cu^{I}$.[23] This seems to be possible via transient coordination of Dp44mT to $Cu^{I}$ and a fast re-oxidation by $O_2$. Based on our combined spectroscopic and computational investigations, we posit

that the acceleration of $Cu^{II}$-Dp44mT reduction by GSH at lower pH is due to a higher population of the $N^2$-protonated complex at low pH. This protonation lowers the affinity to $Cu^{II}$, facilitates the reduction to $Cu^{I}$ via partial de-coordination and hence accelerates the rate-limiting step.

The ability of $Cu^{II}$-Dp44mT to catalyse GSH oxidation at lower pH is not only intriguing and quite exceptional from the chemical point of view but also can be of biological and medicinal interest. Indeed, Dp44mT and its analogues are well-studied anticancer agents that seem to accumulate in the lysosome as $Cu^{II}$-Dp44mT complex and induce lysosomal membrane permeabilization, leading to cell death. Lysosomes have a low pH (~ 4–5.5) and contain thiols, needed to reduce the disulphide bonds of the proteins to digest. There are also no constitutional proteins with high Cu affinity known that could compete Cu out of Dp44mT in the lysosome.[25] Hence, the lysosomal environment would be very favourable for fast thiol oxidation and concomitant ROS production. Here, we showed that the impairment of lysosomal acidification counteracts the cytotoxic activity of $Cu^{II}$-Dp44mT, suggesting that its localization and potential catalytic thiol oxidation in lysosomes play a role in the mode of action.

## Experimental section

### *Materials*

All solvents and reagents obtained from commercial suppliers were used without further purification. TSCs were prepared as previously reported.[26]

### *Preparation of stock solutions*

TSC stock solutions were prepared in DMSO, and their concentration was verified via spectrophotometric $Cu^{II}$ titrations. $Cu^{II}$ stock solution was prepared dissolving $CuCl_2 \cdot 2H_2O$ in ultrapure water ($\rho$ = 18.2 $M\Omega \cdot cm^{-1}$) and its concentration was verified by UV-vis spectroscopy ($\varepsilon_{780}$ = 12 $M^{-1}cm^{-1}$). A stock solution of HEPES buffer (500 mM, pH 7.4) was prepared by dissolving free acid powder in ultrapure water and adjusting the pH with NaOH. A stock solution of MES buffer (500 mM, pH 5) was prepared by dissolving MES sodium salt in ultrapure water and adjusting the pH with HCl. GSH stock solutions were prepared in ultrapure water on a daily basis. TEMPOL stock solution was prepared in ultrapure water.

### *UV-vis spectroscopy*

UV-vis spectra were recorded in 1 cm path quartz cuvettes using an Agilent Cary 60 spectrophotometer. The reaction of $Cu^{II}$-TSC complexes with GSH was performed by adding a small

aliquot of a concentrated GSH solution to the pre-formed $Cu^{II}$-TSC complex in the buffer. For the anaerobic reduction, solutions were thoroughly degassed under $N_2$ before and after the insertion into a sealable cuvette equipped with a pierceable septum, through which GSH was added with a micro-syringe. pH titrations were conducted by adding small aliquots of NaOH solutions to the ligand/complex solution in HCl ~0.01 M. GSH oxidation by $Cu^{II}$-Ap44mT/PTSC complexes was monitored via absorbance change at 254 nm using a ClarioStar plate reader inside a microwell plate.

*HPLC and LC-MS*

HPLC analysis of GSH and GSSG was performed using a Hitachi Primaide instrument on a C18 column (XBridge Peptide BEH C18 column from Waters, 4.6 mm x 150 mm, pore size 300 Å, particle size 3.5 μm) using 0.1% aqueous TFA (solvent A) and 90% $CH_3CN$/0.1% TFA in water (solvent B) with a linear gradient from 5% to 10% solvent B in 7 min. The attribution of the peaks was achieved by comparison with a solution containing GSH or GSSG only, and via LC-MS spectra that were recorded using an LCQ Fleet ion trap mass spectrometer (Thermo Fischer) coupled to a Ultimate3000 RSLCnano system equipped with an ACQUITY UPLC BEH C18 column (130 Å, 1.7 μm, 1.0x150 mm).

*Raman Spectroscopy*

Raman spectra were recorded on a Renishaw inVia Raman microscope equipped with a CCD (charge-coupled device) detector. We used the 457 nm line of an argon laser focused on the sample solution with a 20X objective. Ten accumulations were averaged with an exposure time of 10 s for each sample. The collected data are smoothed with a 13-point Savitzky-Golay $2^{nd}$ order polynomial function.

*EPR spin scavenging*

EPR spin scavenging experiments were performed at room temperature (T = 295 ± 1K) using an EMX-plus (Bruker Biospin GmbH, Germany) X-band EPR spectrometer equipped with a high sensitivity resonator (4119HS-W1, Bruker). The g factor was calibrated in the experimental conditions using the Bruker strong pitch (g = 2.0028). Samples were introduced into glass capillaries (Hirschmann, 25 μL) sealed at both the ends and rapidly transferred into the EPR cavity for measurement. The principal experimental parameters were microwave frequency of ~9.85 GHz, microwave power of ~4.5 mW, modulation amplitude 1 G, time constant of ~5 ms, conversion time of ~12.5 ms. A scan (sweeping time of ~10 s) was then acquired every 17 s to obtain the kinetics of TEMPOL reduction over time. All spectra were best simulated and the resulting simulations were doubly integrated to relatively quantify the concentration of remaining TEMPOL. Data analysis and

simulations based on experimental data were performed using Xenon (Bruker Biospin GmbH, Germany) and lab-made routines based on Easyspin Toolbox under Matlab (Mathworks) environment.[27] The initial decay of TEMPOL EPR intensity was linearly fitted to estimate the $HO^{\bullet}$ production rate (slope of the fitted curves).

*DFT calculations*

All the calculations were carried out by means of the Gaussian16 software package[28] in the context of DFT and its TD-DFT extension. The hybrid meta functional used for geometry optimizations and frequency calculations is M05.[29] Such a functional was employed because it accurately models metallic interactions.[30] Within the frequency calculations, the number of imaginary frequencies, 0 or 1, has been taken into account to confirm the nature of minima and transition states. In the case of the transition states, intrinsic reaction coordinate calculations (IRC) were performed to verify that the imaginary frequency corresponds to the proper motion along the reaction coordinate. The standard 6-311G* basis set of Pople was used for Cu, C, N, O, H atoms and 6-311+G* basis set was used for S atoms. The solvation model based on density, SMD, was adopted in geometry optimizations for mimicking solvent effects using water as the solvent, because it can be consistently used for any charged or uncharged solute in any solvent or liquid medium.[31] To reduce the computational costs and to simulate the thiol-rich environment in which the reaction occurs, cysteine was used instead of GSH to explore the reaction mechanism. Relative Gibbs free energies ($\Delta G$), including thermal corrections at 298.15 K, were calculated for all the located stationary points of the path by with respect to the zero reference energy that is the sum of the energies of separated reactants.

Absorption spectra in an aqueous solution (SMD solvent model) have been calculated, by performing 50 electronic excitations, through the TD-DFT approach. Several computational protocols have been tested for the calculation of the UV-Vis absorption spectra in water and for the calculation of Raman spectra vibrational frequencies to obtain a better agreement with the experimental counterpart. The B3LYP functional[32] has been chosen as the better performing, together with the Pople basis set already used for the geometry optimization. To take into account nonbonding interactions, Grimme dispersion correction has been included using atom pairwise additive scheme,[33] DFT-D3 method.

*MTT viability measurement*

For the viability measurements, the human colon carcinoma cell models SW480 (obtained from ATCC) were used and cultured at 37 °C and 5% $CO_2$, in MEME (Merck, M0268) medium, respectively, supplemented with 10% fetal calf serum (PAA, Austria). Cells were plated ($2 \times 10^3$ cells/well) in 96-well plates and allowed to recover for 24 h. Then, cells were pre-treated with 0, 1, 2.5, 5, 7.5 and 10 nM bafilomycin A1 for 1h. After which, increasing concentrations of Dp44mT or

its copper complex were added for 48 h. Cell viability was measured by the 3-(4,5-dimethylthiazol-2-yl)-2,5-diphenyltetrazolium bromide (MTT)-based vitality assay (EZ4U; Biomedica, Vienna, Austria). Combination indices were calculated by CalcuSyn using the Chou-Talalay method.[34] Values above 1 indicate antagonism and values below 1 synergism.

**Acknowledgement**

We acknowledge financial support from the French National Research Agency (ANR) through the 17-EURE-0016 and CHAPCOP-ANR-19-CE44-0018 programs, the University of Calabria and the City of Vienna Fund for Innovative Interdisciplinary Cancer Research (21134).

**References**

(1) Schafer, F. Q.; Buettner, G. R. Redox environment of the cell as viewed through the redox state of the glutathione disulfide/glutathione couple. *Free radical biology and medicine* **2001**, *30* (11), 1191-1212.

(2) Jungwirth, U.; Kowol, C. R.; Keppler, B. K.; Hartinger, C. G.; Berger, W.; Heffeter, P. Anticancer activity of metal complexes: involvement of redox processes. *Antioxid Redox Signal* **2011**, *15* (4), 1085-1127. DOI: 10.1089/ars.2010.3663 From NLM.

(3) Heffeter, P.; Jungwirth, U.; Jakupec, M.; Hartinger, C.; Galanski, M.; Elbling, L.; Micksche, M.; Keppler, B.; Berger, W. Resistance against novel anticancer metal compounds: differences and similarities. *Drug Resist Updat* **2008**, *11* (1-2), 1-16. DOI: 10.1016/j.drup.2008.02.002 From NLM.

Valente, A.; Podolski-Renić, A.; Poetsch, I.; Filipović, N.; López, Ó.; Turel, I.; Heffeter, P. Metal- and metalloid-based compounds to target and reverse cancer multidrug resistance. *Drug Resist Updat* **2021**, *58*, 100778. DOI: 10.1016/j.drup.2021.100778 From NLM.

(4) Desideri, E.; Ciccarone, F.; Ciriolo, M. R. Targeting glutathione metabolism: Partner in crime in anticancer therapy. *Nutrients* **2019**, *11* (8), 1926.

(5) Jocelyn, P. C. The standard redox potential of cysteine-cystine from the thiol-disulphide exchange reaction with glutathione and lipoic acid. *European journal of biochemistry* **1967**, *2* (3), 327-331.

(6) Winther, J. R.; Thorpe, C. Quantification of thiols and disulfides. *Biochimica et Biophysica Acta (BBA)-General Subjects* **2014**, *1840* (2), 838-846.

(7) Smith, R. C.; Reed, V. D. Hill WE Oxidation Of Thiols By Copper (II) Phosphorus. *Sulfur. Silicon Relat. Elem* **1994**, *90*, 147-154.

(8) Guo, Z.-L.; Richardson, D. R.; Kalinowski, D. S.; Kovacevic, Z.; Tan-Un, K. C.; Chan, G. C.-F. The novel thiosemicarbazone, di-2-pyridylketone 4-cyclohexyl-4-methyl-3-thiosemicarbazone (DpC), inhibits neuroblastoma growth in vitro and in vivo via multiple mechanisms. *Journal of Hematology & Oncology* **2016**, *9* (1), 98. Gutierrez, E. M.; Seebacher, N. A.; Arzuman, L.; Kovacevic, Z.; Lane, D. J. R.; Richardson, V.; Merlot, A. M.; Lok, H.; Kalinowski, D. S.; Sahni, S. Lysosomal membrane stability plays a major role in the cytotoxic activity of the anti-proliferative agent, di-2-pyridylketone 4, 4-dimethyl-3-thiosemicarbazone (Dp44mT). *Biochimica et Biophysica Acta (BBA)-Molecular Cell Research* **2016**, *1863* (7), 1665-1681.

(9) Lovejoy, D. B.; Jansson, P. J.; Brunk, U. T.; Wong, J.; Ponka, P.; Richardson, D. R. Findings define a novel generalized strategy to target cancer cells by disrupting lysosome function in a selective manner that is associated with apoptosis induction and potent antitumor effects. *Cancer Research* **2011**.

(10) Stacy, A. E.; Palanimuthu, D.; Bernhardt, P. V.; Kalinowski, D. S.; Jansson, P. J.; Richardson, D. R. Zinc(II)–Thiosemicarbazone Complexes Are Localized to the Lysosomal Compartment Where They Transmetallate with Copper Ions to Induce Cytotoxicity. *Journal of Medicinal Chemistry* **2016**, *59* (10), 4965-4984. DOI: 10.1021/acs.jmedchem.6b00238.

(11) Hager, S.; Korbula, K.; Bielec, B.; Grusch, M.; Pirker, C.; Schosserer, M.; Liendl, L.; Lang, M.; Grillari, J.; Nowikovsky, K. The thiosemicarbazone Me 2 NNMe 2 induces paraptosis by disrupting the ER thiol redox homeostasis based on protein disulfide isomerase inhibition. *Cell death & disease* **2018**, *9* (11), 1-17.

(12) Heffeter, P.; Pape, V. F. S.; Enyedy, É. A.; Keppler, B. K.; Szakacs, G.; Kowol, C. R. Anticancer thiosemicarbazones: chemical properties, interaction with iron metabolism, and resistance development. *Antioxidants & redox signaling* **2019**, *30* (8), 1062-1082. Dömötör, O.; May, N. V.; Pelivan, K.; Kiss, T.; Keppler, B. K.; Kowol, C. R.; Enyedy, É. A. A comparative study of α-N-pyridyl thiosemicarbazones: Spectroscopic properties, solution stability and copper (II) complexation. *Inorganica Chimica Acta* **2018**, *472*, 264-275. Enyedy, É. A.; Nagy, N. V.; Zsigó, É.; Kowol, C. R.; Arion, V. B.; Keppler, B. K.; Kiss, T. Comparative Solution Equilibrium Study of the Interactions of Copper (II), Iron (II) and Zinc (II) with Triapine (3-Aminopyridine-2-carbaldehyde Thiosemicarbazone) and Related Ligands. WILEY-VCH Verlag Weinheim: 2010.

(13) Kallus, S.; Uhlik, L.; van Schoonhoven, S.; Pelivan, K.; Berger, W.; Enyedy, É. A.; Hofmann, T.; Heffeter, P.; Kowol, C. R.; Keppler, B. K. Synthesis and biological evaluation of biotin-conjugated anticancer thiosemicarbazones and their iron (III) and copper (II) complexes. *Journal of inorganic biochemistry* **2019**, *190*, 85-97. Bernhardt, P. V.; Sharpe, P. C.; Islam, M.; Lovejoy, D. B.; Kalinowski, D. S.; Richardson, D. R. Iron chelators of the dipyridylketone thiosemicarbazone class: precomplexation and transmetalation effects on anticancer activity. *Journal of medicinal chemistry* **2009**, *52* (2), 407-415. Kowol, C. R.; Heffeter, P.; Miklos, W.; Gille, L.; Trondl, R.; Cappellacci, L.; Berger, W.; Keppler, B. K. Mechanisms underlying reductant-induced reactive oxygen species formation by anticancer copper (II) compounds. *JBIC Journal of Biological Inorganic Chemistry* **2012**, *17* (3), 409-423.

(14) Hager, S.; Pape, V. F. S.; Pósa, V.; Montsch, B.; Uhlik, L.; Szakács, G.; Tóth, S.; Jabronka, N.; Keppler, B. K.; Kowol, C. R. High copper complex stability and slow reduction kinetics as key parameters for improved activity, paraptosis induction, and impact on drug-resistant cells of anticancer thiosemicarbazones. *Antioxidants & redox signaling* **2020**, *33* (6), 395-414.

(15) Santoro, A.; Vileno, B.; Palacios, Ò.; Peris-Díaz, M. D.; Riegel, G.; Gaiddon, C.; Krężel, A.; Faller, P. Reactivity of Cu (ii)–, Zn (ii)–and Fe (ii)–thiosemicarbazone complexes with glutathione

and metallothionein: from stability to dissociation to transmetallation. *Metallomics* **2019**, *11* (5), 994-1004.

(16) Huyghues-Despointes, B. M. P.; Nelson, J. W. Measurements of disulfide bond stabilities in protein folding intermediates. *Measurements of disulfide bond stabilities in protein folding intermediates.* **1990**, 457-466.

(17) Takeshita, K.; Saito, K.; Ueda, J.-i.; Anzai, K.; Ozawa, T. Kinetic study on ESR signal decay of nitroxyl radicals, potent redox probes for in vivo ESR spectroscopy, caused by reactive oxygen species. *Biochimica et Biophysica Acta (BBA)-General Subjects* **2002**, *1573* (2), 156-164.

(18) Bagiyan, G. A.; Koroleva, I. K.; Soroka, N. V.; Ufimtsev, A. V. Kinetics of the catalytic oxidation reactions of thiol compounds in aqueous solutions in the presence of copper ions. *Kinetics and catalysis* **2004**, *45* (3), 372-380. Bagiyan, G. A.; Koroleva, I. K.; Soroka, N. V.; Ufimtsev, A. V. Oxidation of aminothiols by molecular oxygen catalyzed by copper ions. Stoichiometry of the reaction. *Russian chemical bulletin* **2003**, *52* (5), 1129-1134.

(19) Ufnalska, I.; Drew, S. C.; Zhukov, I.; Szutkowski, K.; Wawrzyniak, U. E.; Wróblewski, W.; Frączyk, T.; Bal, W. Intermediate Cu (II)-Thiolate Species in the Reduction of Cu (II) GHK by Glutathione: A Handy Chelate for Biological Cu (II) Reduction. *Inorganic Chemistry* **2021**.

(20) Anderson, C. H.; Holwerda, R. A. Mechanistic flexibility in the reduction of copper(II) complexes of aliphatic polyamines by mercapto amino acids. *J Inorg Biochem* **1985**, *23* (1), 29-41. DOI: 10.1016/0162-0134(84)85003-5 From NLM. Calvo, J. S.; Villones, R. L. E.; York, N. J.; Stefaniak, E.; Hamilton, G. E.; Stelling, A. L.; Bal, W.; Pierce, B. S.; Meloni, G. Evidence for a Long-Lived, Cu-Coupled and Oxygen-Inert Disulfide Radical Anion in the Assembly of Metallothionein-3 Cu(I)(4)-Thiolate Cluster. *J Am Chem Soc* **2022**, *144* (2), 709-722. DOI: 10.1021/jacs.1c03984 From NLM.

(21) Weik, M.; Bergès, J.; Raves, M. L.; Gros, P.; McSweeney, S.; Silman, I.; Sussman, J. L.; Houée-Levin, C.; Ravelli, R. B. Evidence for the formation of disulfide radicals in protein crystals upon X-ray irradiation. *J Synchrotron Radiat* **2002**, *9* (Pt 6), 342-346. DOI: 10.1107/s0909049502014589 From NLM. Antonello, S.; Daasbjerg, K.; Jensen, H.; Taddei, F.; Maran, F. Formation and cleavage of aromatic disulfide radical anions. *J Am Chem Soc* **2003**, *125* (48), 14905-14916. DOI: 10.1021/ja036380g From NLM. Dumont, E.; Laurent, A. D.; Assfeld, X. Intersulfur Distance Is a Key Factor in Tuning Disulfide Radical Anion Vertical UV−Visible Absorption. *The Journal of Physical Chemistry Letters* **2010**, *1* (2), 581-586. DOI: 10.1021/jz900214e.

(22) Yoshimori, T.; Yamamoto, A.; Moriyama, Y.; Futai, M.; Tashiro, Y. Bafilomycin A1, a specific inhibitor of vacuolar-type H(+)-ATPase, inhibits acidification and protein degradation in lysosomes of cultured cells. *J Biol Chem* **1991**, *266* (26), 17707-17712. From NLM.

(23) Morgan, M. T.; Nguyen, L. A. H.; Hancock, H. L.; Fahrni, C. J. Glutathione limits aquacopper (I) to sub-femtomolar concentrations through cooperative assembly of a tetranuclear cluster. *Journal of Biological Chemistry* **2017**, *292* (52), 21558-21567.
(24) Allen, R. N.; Shukla, M. K.; Reed, D.; Leszczynski, J. Ab initio study of the structural properties of ascorbic acid (vitamin C). *International journal of quantum chemistry* **2006**, *106* (14), 2934-2943.
(25) Polishchuk, E. V.; Polishchuk, R. S. The emerging role of lysosomes in copper homeostasis. *Metallomics* **2016**, *8* (9), 853-862.
(26) Kowol, C. R.; Trondl, R.; Heffeter, P.; Arion, V. B.; Jakupec, M. A.; Roller, A.; Galanski, M.; Berger, W.; Keppler, B. K. Impact of metal coordination on cytotoxicity of 3-aminopyridine-2-carboxaldehyde thiosemicarbazone (triapine) and novel insights into terminal dimethylation. *J Med Chem* **2009**, *52* (16), 5032-5043. DOI: 10.1021/jm900528d From NLM. Lovejoy, D. B.; Sharp, D. M.; Seebacher, N.; Obeidy, P.; Prichard, T.; Stefani, C.; Basha, M. T.; Sharpe, P. C.; Jansson, P. J.; Kalinowski, D. S.; et al. Novel second-generation di-2-pyridylketone thiosemicarbazones show synergism with standard chemotherapeutics and demonstrate potent activity against lung cancer xenografts after oral and intravenous administration in vivo. *J Med Chem* **2012**, *55* (16), 7230-7244. DOI: 10.1021/jm300768u From NLM.
(27) Stoll, S.; Schweiger, A. EasySpin, a comprehensive software package for spectral simulation and analysis in EPR. *Journal of magnetic resonance* **2006**, *178* (1), 42-55.
(28) Frisch, M. J.; Trucks, G. W.; Schlegel, H. B.; Scuseria, G. E.; Robb, M. A.; Cheeseman, J. R.; Scalmani, G.; Barone, V.; Petersson, G. A.; Nakatsuji, H. Gaussian 16, Revision C. 01. Gaussian, Inc., Wallingford CT. 2016. *Google Scholar There is no corresponding record for this reference* **2020**.
(29) Zhao, Y.; Schultz, N. E.; Truhlar, D. G. Design of density functionals by combining the method of constraint satisfaction with parametrization for thermochemistry, thermochemical kinetics, and noncovalent interactions. *Journal of Chemical Theory and Computation* **2006**, *2* (2), 364-382.
(30) Zhao, Y.; Schultz, N. E.; Truhlar, D. G. Exchange-correlation functional with broad accuracy for metallic and nonmetallic compounds, kinetics, and noncovalent interactions. *The Journal of chemical physics* **2005**, *123* (16), 161103.
(31) Marenich, A. V.; Cramer, C. J.; Truhlar, D. G. Universal solvation model based on solute electron density and on a continuum model of the solvent defined by the bulk dielectric constant and atomic surface tensions. *The Journal of Physical Chemistry B* **2009**, *113* (18), 6378-6396.
(32) Becke, A. D. Becke's three parameter hybrid method using the LYP correlation functional. *J. Chem. Phys* **1993**, *98* (492), 5648-5652. Lee, C.; Yang, W.; Parr, R. G. Development of the Colle-

Salvetti conelation energy formula into a functional of the electron density. *Phys. Rev, vol. B* **1988**, *37*, 785-789.

(33) Grimme, S.; Antony, J.; Ehrlich, S.; Krieg, H. A consistent and accurate ab initio parametrization of density functional dispersion correction (DFT-D) for the 94 elements H-Pu. *The Journal of chemical physics* **2010**, *132* (15), 154104.

(34) Chou, T.-C. Drug Combination Studies and Their Synergy Quantification Using the Chou-Talalay Method. *Cancer Research* **2010**, *70* (2), 440-446. DOI: 10.1158/0008-5472.CAN-09-1947 (acccessed 4/28/2022).